Anal. Chem. **2002,** *74,* 992−1006

Coupling Ion Mobility Separations, Collisional Activation Techniques, and Multiple Stages of MS for Analysis of Complex Peptide Mixtures

Cherokee S. Hoaglund-Hyzer,† Young Jin Lee, Anne E. Counterman, and David E. Clemmer*

Department of Chemistry, Indiana University, Bloomington IN, 47405

An ion trap/ion mobility/quadrupole/collision cell/time-of-flight mass spectrometer that incorporates a differentially pumped orifice-skimmer cone region at the back of the drift tube has been developed for the analysis of peptide mixtures. The combined approach allows a variety of strategies to be employed for collisionally activating ions, and fragments can be monitored by subsequent stages of mass spectrometry in a parallel fashion, as described previously (*Anal. Chem.* 2000, *72,* 2737). Here, we describe the overall experimental approach in detail. Applications involving different aspects of the initial mobility separation and various collisional activation and parallel sequencing strategies are illustrated by examining several simple peptide mixtures and a mixture of tryptic peptides from *β*-casein. Detection limits associated with various experimental configurations and the utility for analysis of complex systems are discussed.

During the past 10 years, there has been substantial progress in the development of techniques related to ion mobility spectrometry (IMS).[1] This can be largely attributed to the incorporation of new ion sources[2,3] for mass spectrometry (MS) and the development of sophisticated theoretical computation methods for generating candidate ion geometries[4,5] and subsequent calculation of their mobilities.[6] The latter work allows IMS data to be used as a structural probe, and rich areas related to understanding the geometries of small clusters[7] and synthetic polymers[8] and the conformations of anhydrous[9] or partially solvated[10] biomolecular ions have emerged.

Our group has worked to extend ion mobility separation techniques for the analysis of complex mixtures.[11−14] To this end, we have developed several technologies based on a combination of techniques that include electrospray ionization (ESI),[2] IMS, and several types of MS techniques including quadrupole,[15] ion trap,[16,17] and time-of-flight[18] mass analyzers. For example, the combination of IMS with time-of-flight (TOF) MS can be accomplished such that flight times in the mass spectrometer (which

† Current address: Eli Lilly & Co., Indianapolis, IN 46285.

(1) See, for example: Tou, J. C.; Boggs, G. U. *Anal. Chem.* **1976**, *48*, 351. Hagen, D. F. *Anal. Chem.* **1979**, *51*, 870. Hill, H. H.; Siems, W. F.; St. Louis, R. H.; McMinn, D. G. *Anal. Chem.* **1990**, *62*, 1201A. St. Louis, R. H.; Hill, H. H. *Crit. Rev. Anal. Chem.* **1990**, *21*, 321. von Helden, G.; Hsu, M.-T.; Kemper, P. R.; Bowers, M. T. *J. Chem. Phys.* **1991**, *95*, 3835. Jarrold, M. F. *J. Phys. Chem.* **1995**, *99*, 11. Clemmer, D. E.; Jarrold, M. F. *J. Mass Spectrom.* **1997**, *32*, 577.

(2) Fenn, J. B.; Mann, M.; Meng, C. K.; Wong, S. F.; Whitehouse, C. M. *Science* **1989**, *246*, 64.

(3) Karas, M.; Hillenkamp, F. *Anal. Chem.* **1988**, *60*, 2299.

(4) Molecular modeling software by Insight II, BIOSYM/MSI: San Diego, CA 1995.

(5) A number of force fields, including several variations of AMBER, CHARMM, CVFF, and GROMOS, have been used to generate trial in vacuo conformations for comparison to experimental results. Wiener, S. J.; Kollman, P. A.; Nguyen, D. T.; Case, D. A. *J. Comput. Chem.* **1986**, *7*, 230; Lazardis, T.; Archontis, G.; Karplus, M. *Adv. Protein Chem.* **1995**, *47*, 231; Dauber-Osguthorpe, P.; Roberts, V. A.; Osguthorpe, D. J.; Wolff, J.; Genest, M.; Hagler, A. T. *Proteins: Struct., Funct., Genet.* **1988**, *4*, 31. van Gunsteren, W. F.; Berendsen, H. J. *Groningen Molecular Simulation (GROMOS) Library Manual* Biomos, Nijenborgh 16, 9747 AG Groiningen, The Netherlands, 1987.

(6) See, for example: Jarrold, M. F.; Constant, V. A. *Phys. Rev. Lett.* **1991**, *67*, 2994. Wyttenbach, T.; von Helden, G.; Batka, J. J., Jr.; Carlat, D.; Bowers, M. T. *J. Am. Soc. Mass Spectrom.* **1997**, *8*, 275. Mesleh, M. F.; Hunter, J. M.; Shvartsburg, A. A.; Schatz, G. C.; Jarrold, M. F. *J. Phys. Chem.* **1996**, *100*, 16082; Shvartsburg, A. A.; Jarrold, M. F. *Chem. Phys. Lett.* **1996**, *261*, 86.

(7) Jarrold, M. F.; Bower, J. E.; Creegan, K. *J. Chem. Phys.* **1989**, *90*, 3615.

(8) See, for example: von Helden, G.; Wyttenbach, T.; Bowers. M. T. *Science* **1995**, *267*, 1483. Wyttenbach, T.; von Helden, G.; Bowers. M. T. *Int. J. Mass Spectrom. Ion Processes* **1997**, *165/166*, 377. Gidden, J.; Wyttenbach, T.; Batka, J. J.; Weis, P.; Jackson, A. T.; Scrivens, J. H.; Bowers, M. T. *J. Am. Chem. Soc.* **1999**, *121*, 1421. Gidden, J.; Wyttenbach, T.; Batka, J. J.; Weis, P.; Jackson, A. T.; Scrivens, J. H.; Bowers, M. T. *J. Am. Soc. Mass. Spectrom.* **1999**, *10*, 883.

(9) Hoaglund Hyzer, C. S.; Counterman, A. E.; Clemmer, D. E. *Chem. Rev.* **1999**, *99*, 3037 and references therein.

(10) Lau, Y. K.; Ikuta, S.; Kebarle, P. *J. Am. Chem. Soc.* **1982**, *104*, 1462. Klassen, J. S.; Blades, A. T.; Kebarle, P. *J. Phys. Chem.* **1995**, *99*, 15509. Woenckhaus, J.; Hudgins, R. R.; Jarrold, M. F. *J. Am. Chem. Soc.* **1997**, *119*, 9586. Fye, J. L.; Woenckhaus, J.; Jarrold, M. F. *J. Am. Chem. Soc.* **1998**, *120*, 1327.

(11) Srebalus, C. A.; Li, J.; Marshall, W. S.; Clemmer, D. E. *Anal. Chem.* **1999**, *71*, 3918.

(12) Srebalus, C. A.; Li, J.; Marshall, W. S.; Clemmer, D. E. *J. Am. Soc. Mass Spectrom.* **2000**, *11*, 352.

(13) Srebalus Barnes, C. A.; Clemmer, D. E. *Anal. Chem.* **2001**, *73*, 424.

(14) Zientara, G. A.; Taraszka, J. A.; Kindy, J. M.; Clemmer, D. E. Work in progress.

(15) Miller, P. E.; Denton, M. B. *J. Chem. Educ.* **1986**, *63*, 617. Dawson, P. H., ed. *Quadrupole Mass Spectrometry and its Applications*; Woodbury: AIP Press: Secaucus, NJ, 1995. Konenkov, N. V.; Kratenko, V. I. *Int. J. Mass Spectrom. Ion Processes* **1991**, *108*, 115.

(16) March, R.; Huges, R. *Quadrupole Storage Mass Spectrometry*; Wiley: New York, 1989. Cooks, R. G.; Kaiser, R. E., Jr. *Acc. Chem. Res.* **1990**, *23*, 213. Glish, G. L.; McLuckey, S. A. *Int. J. Mass Spectrom. Ion Processes* **1991**, *106*, 1. March, R. E. *J. Mass Spectrom.* **1997**, *32*, 351.

(17) The ion trap/IMS interface for ESI that we have developed is similar to interfaces for TOF described in: Michael, S. M.; Chien, M.; Lubman, D. M. *Rev. Sci. Instrum.* **1992**, *63* (10), 4277. Michael, S. M.; Chien, B. M.; Lubman, D. M. *Anal. Chem.* **1993**, *65*, 2614. Quian, M. G.; Lubman, D. M. *Anal. Chem.* **1995**, *67*, 234A.

(18) Cotter, R. J. *Time-of-Flight Mass Spectrometry*; American Chemical Society: Washington, DC, 1997. Standing, K. G. *Int. J. Mass Spectrom.* **2000**, *200*, 597.

10.1021/ac010837s CCC: $22.00
Published on Web 02/02/2002

by design occur on microsecond time scales) are recorded within individual drift time windows (usually 10−30 μs) associated with the mobility measurement.[19] We refer to this as a "nested" drift-(flight) time measurement. The ability to disperse mixtures of ions in two gas-phase dimensions on millisecond time scales is appealing for several reasons. When applied to complex mixtures, the mobility separation reduces congestion in mass spectra and provides complementary information about charge state and cross section that can be used for assignment of peaks to expected components. We have previously demonstrated the utility of these methodologies in the analysis of complex mixtures of peptides and proteins, such as those that arise in combinatorial libraries[11−13] and cellular proteomes.[14] The millisecond time scale of the gas-phase separation is also sufficiently short that it can be coupled with traditional liquid chromatography (LC) separations that occur over seconds to minutes.[20,21]

Another advantage comes about by incorporating a collision cell between the drift tube and TOF instruments.[22] In this configuration, as mobility-separated ions exit the drift tube, they are exposed to energizing collisions, and the fragments that are formed are recorded at drift times that are coincident with their antecedent parents. This strategy, in which fragments are effectively "labeled" according to the drift time of the corresponding parent ion, allows the acquisition of fragmentation mass spectra for multiple parent ions in a parallel fashion. Recently, we have incorporated a quadrupole mass filter (Q) with the collision cell, an IMS/Q/TOF approach.[23] This approach allows fragments to be unambiguously assigned to a specific m/z-selected parent ion, even when two parent ions have identical mobilities.[22]

In this paper, we extend the IMS/Q/TOF technique by incorporating a differentially pumped orifice-skimmer cone (OSC) region at the back of the drift tube.[2] With this approach, it is possible to separate a distribution of parent ions in the drift tube and generate mobility-separated primary (1°) fragments in the OSC region before ions enter the quadrupole mass filter. A 1° fragment can be selected with the mass filter and collisionally activated again in a collision cell to generate a distribution of secondary (2°) fragments, which are then dispersed into a TOF instrument for mass analysis. By paying careful attention to the time requirements for the separation and activation processes, it is possible to retain information about the original parent ion mobilities. The approach is designed to circumvent a fundamental limitation that arises with combinations of IMS and MS technologies: mobility and m/z ratios are not orthogonal properties. That is, the size of an ion is related to its mass. By breaking the parent ions apart, it is possible to generate 1° fragments with m/z ratios that are effectively independent of the parent ion mobility. Many fragments are then situated at positions in the data arrays that allow them to be easily mass-selected. Subsequent dissociation of the 1° fragments can be used to identify the original parents. The instrument that is used for these studies is flexible and can be operated in a variety of configurations. Here, we demonstrate a number of different approaches by examining a mixture that arises from a tryptic digest, as well as several carefully prepared peptide systems. The latter mixtures allow us to assess the detection limits of various configurations.

The techniques and experiments described below are related to other work involving the separation of ions in gases. Hill[25] and Jarrold[26] have developed high-resolution drift tubes with ESI sources for the analysis of biomolecular systems. Bowers's group has recently developed an ESI drift tube approach that incorporates an ion funnel.[27] The funnel increases transmission in the source and can be used to accumulate ions, similarly to the ion trap interface developed by Hoaglund et al.[38] Bowers's group has also developed several instruments that incorporate a matrix assisted laser desorption ionization (MALDI) source,[28] an approach that has subsequently been used by Russell and his collaborators.[29] Russell's group has also incorporated surface-induced dissociation (SID)[30] between IMS and TOF instruments.[31] Several other strategies that take advantage of ion interactions with inert buffer gases for isolation of different structures are also under development. Cooks and co-workers have examined collisional dampening profiles in ion traps in order to resolve isobaric species and have reported derived collision cross sections for these data.[32] Guevremont's group has developed the field asymmetric ion mobility spectrometry (FAIMS) method[33] that separates ions based on differences in low- and high-field mobilities. They have shown that it is possible to separate different conformers of proteins[34] and that the technique can enhance ion transmission through the ESI source.[35]

EXPERIMENTAL

Overview of Instrument and General Experimental Approach. Figure 1 shows a schematic diagram of the instrument. The ion trap and injected-ion drift tube are housed in a large vacuum chamber that is pumped by two Edwards ISO-250 diffusion pumps (2000 L sec^{-1}). An adjoining chamber is split into

(19) Hoaglund, C. S.; Valentine, S. J.; Sporleder, C. R.; Reilly, J. P.; Clemmer, D. E. *Anal. Chem.* **1998**, *70*, 2236.
(20) Valentine, S. J.; Kulchania, M.; Srebalus Barnes, C. A.; Clemmer, D. E. *Int. J. Mass Spectrom.* **2001**, *212* (1−3), 97.
(21) Srebalus Barnes, C. A.; Hilderbrand A. E.; Valentine, S. J.; Clemmer, D. E. *Anal. Chem.* **2002**, *74*, 26.
(22) Hoaglund-Hyzer, C. S.; Li, J.; Clemmer, D. E. *Anal. Chem.* **2000**, *72*, 2737.
(23) Hoaglund-Hyzer, C. S.; Clemmer, D. E. *Anal. Chem.* **2001**, *73*, 177.
(24) Lee, Y. J.; Hoaglund-Hyzer, C. S.; Taraszka, J. A.; Zientara, G. A.; Counterman, A. E.; Clemmer, D. E. *Anal. Chem.* **2001**, *73*, 3549.
(25) Wittmer, D.; Chen, Y. H.; Luckenbill, B. K.; Hill, H. H., Jr. *Anal. Chem.* **1994**, *66*, 2348.; Chen, Y. H.; Hill, H. H., Jr.; Wittmer, D. P. *Int. J. Mass Spectrom. Ion Processes* **1996**, *154*, 1. Wu, C.; Siems, W. F.; Asbury, G. R.; Hill, H. H. Jr. *Anal. Chem.* **1998**, *70*, 4929.
(26) Hudgins, R. R.; Woenckhaus, J.; Jarrold, M. F. *Int. J. Mass Spectrom. Ion Processes* **1997**, *165/166*, 497.
(27) Bowers, M. T., personal communication.
(28) Kemper, P. R.; Bowers, M. T. *J. Am. Soc. Mass Spectrom.* **1990**, *1*, 197. vonHelden, G.; Wyttenbach, T.; Bowers, M. T. *Int. J. Mass Spectrom. Ion Processes* **1995**, *146/147*, 349.
(29) Gillig, K. J.; Ruotolo, B.; Stone, E. G.; Russell, D. H.; Fuhrer, K.; Gonin, M.; Schultz, A. J. *Anal. Chem.* **2000**, *72*, 3965.
(30) Cooks, R. G.; Ast, T.; Mabud, A. *Int. J. Mass Spectrom. Ion Processes* **1990**, *100*, 209.
(31) Stone, E.; Gillig, K. J.; Ruotolo, B.; Fuhrer, K.; Gonin, M.; Schultz, A.; Russell, D. H. *Anal. Chem.* **2001**, *73*, 2233.
(32) Plass, W. R.; Gill, L. A.; Bui, H. A.; Cooks, R. G. *J. Phys. Chem. A* **2000**, *104*, 5059.
(33) Buryakov, I. A.; Krylov, E. V.; Nazarov, E. G.; Rasulev, U. K. *Int. J. Mass Spectrom. Ion Processes* **1993**, *128*, 143.
(34) Purves, R. W.; Barnett, D. A.; Ells, B.; Guevremont, R. *Int. J. Mass Spectrom.* **2000**, *197*, 163. Purves, R. W.; Barnett, D. A.; Ells, B.; Guevremont, R. *J. Am. Soc. Mass Spectrom.* **2000**, *11*, 738. Purves, R. W., Barnett, D. A., Ells, B., Guevremont, R., *J. Am. Soc. Mass Spectrom.* **2001**, *12*, 894.
(35) Barnett, D. A.; Guevremont, R.; Purves, R. W. *Applied Spectroscopy* **1999**, *53*, 1367. Ells, B.; Barnett, D. A.; Purves, R. W.; Guevremont, R. *Anal. Chem.* **2000**, *72*, 4555. McCooeye, M. A.; Ells, B.; Barnett, D. A.; Purves, R. W.; Guevremont, R. *J. Anal. Toxicol.* **2001**, *25*, 81.

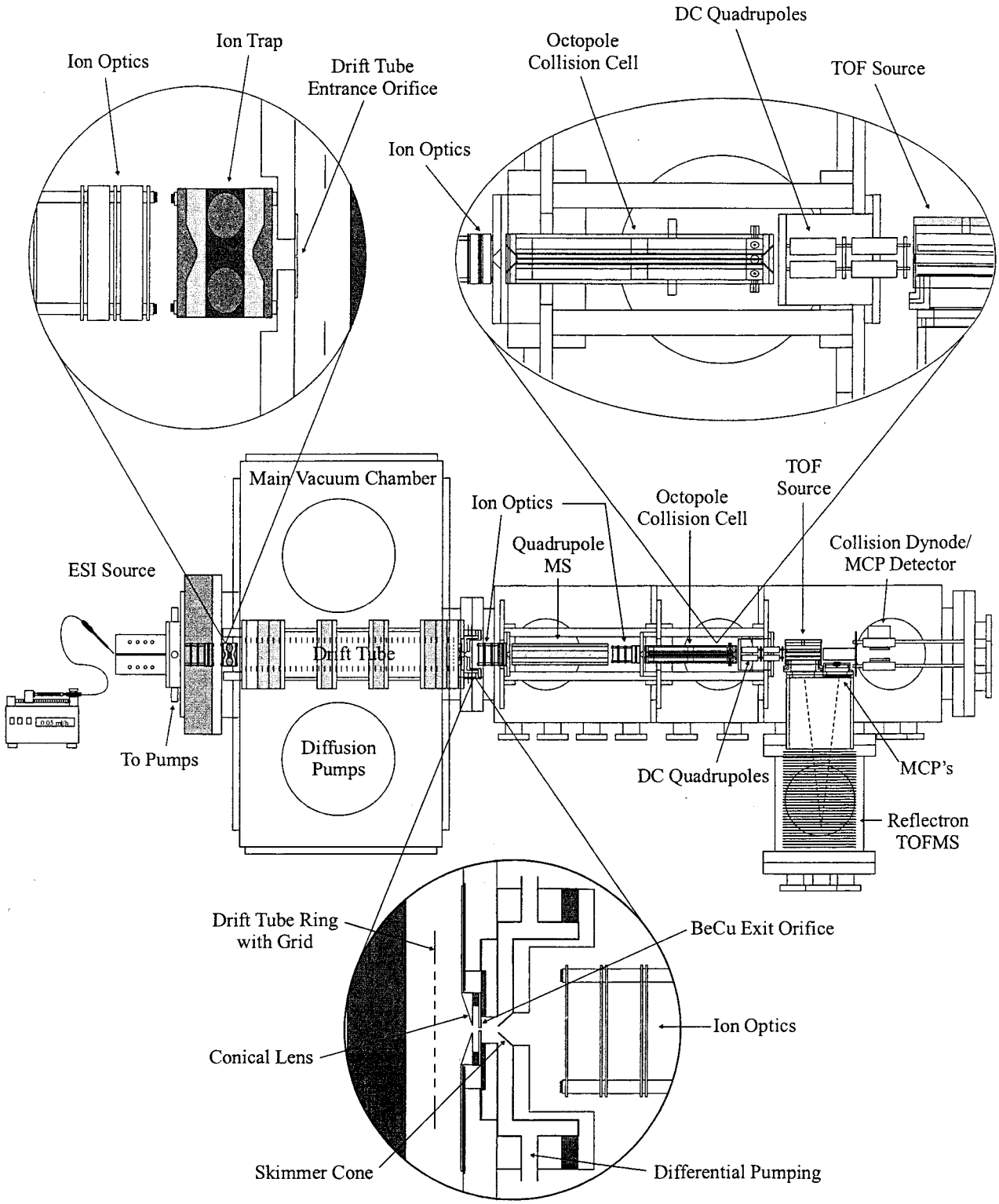

Figure 1. Schematic diagram of the ESI/ion trap/drift tube/quadrupole/octopole collision cell/reflectron time-of-flight mass spectrometer. The insets show the details of the ion trap interface, the differentially pumped orifice-skimmer cone region, and the octopole collision cell. The apparatus is described in detail in the text.

three different sections. The first and second sections, each pumped by an Edwards ISO-160 diffusion pump (700 L s^{-1}), house the quadrupole mass spectrometer and the octopole collision cell, respectively. The last section is pumped by two Edwards ISO-160 diffusion pumps and contains a reflectron time-of-flight mass spectrometer that is situated orthogonal to the beam axis.

Key to the present work is the idea that collisional activation can be carried out at a number of different places in the instrument. We and others have previously discussed the idea that ions can be activated in the ion trap[16] as well as upon high-energy injection into the drift tube.[23,36,37,38] A detailed view of this region is given in the inset of Figure 1. Below, we focus our discussion on dissociation that can be carried out in the orifice

skimmer cone (OSC) region at the end of the drift tube and in the octopole collision cell. Detailed diagrams of these portions of the instrument are also shown in Figure 1. As described in detail below, the ability to separate and fragment ions before m/z selection in the quadrupole has several advantages, primarily that 1° fragments often occur at positions in the spectrum that allow them to be easily selected for subsequent studies.

The general experimental approach is as follows. The continuous beam of electrosprayed ions is extracted into a high-vacuum region and accumulated in the quadrupole ion trap. Experiments are initiated by injecting a short pulse of ions into a drift tube that contains an inert buffer gas (either He or Ar in these experiments). Ions drift through the gas under the influence of a weak uniform electric field and are separated on the basis of differences in their gas-phase mobilities. Ions are extracted from the drift tube using a high-pressure focusing element[24] directly into a differentially pumped OSC region. They are accelerated across this region and subjected to energizing collisions that, depending upon the potential difference used, can induce fragmentation. Ions exit the OSC region into the main vacuum chamber and are focused into a quadrupole mass filter that can be set to transmit all ions or to select specific m/z species. As ions exit the quadrupole, they are decelerated to a desired kinetic energy and injected into an octopole collision cell. The collision cell can be filled with a target gas (usually UHP zero-grade argon, Air Products) for collision-induced dissociation (CID) studies. Parent and fragment ions exit the gas cell and are focused into two sets of dc quadrupoles that shape the beam into a ribbon prior to entering the source region of a reflectron-geometry TOF mass spectrometer.

Ion Accumulation and Injection. Ions from the source are focused into a low-energy beam and guided into an ion trap (R. M. Jordan, model C-1251). The ion trap consists of a center ring (operated at 1.0 MHz and ~3000 V_{pp}) and two end caps that are mounted directly to the entrance plate of the drift tube.[38] The trap operates at $\sim 10^{-4}-10^{-3}$ Torr, supplied from buffer gas that leaks out of the entrance of the drift tube (as well as ambient background gas from the main chamber). Ions are ejected from the trap by turning the rf field off and supplying a short dc pulse (0.6 μs) to one of the end caps. The energy used to inject ions into the drift tube is determined by the potential difference between the trap and the entrance plate of the drift tube, −70 to 130 V in these experiments. During injection, initial collisions with the buffer gas thermalize the ions kinetic energies; further collisions cool them to the buffer gas temperature (300 K).[39,40] Under appropriate conditions (high injection voltages), this heating/cooling cycle can cause fragmentation.[23,36,37,38] Additionally, endothermic proton transfer may occur.[41]

Drift Tube, Focusing Element, and Differentially Pumped OSC Region. The drift tube is 50.6 cm long and can be operated with ~1.0−5.0 Torr of helium or argon buffer gas. The body is composed of five stainless steel sections that are electrically isolated with ceramic spacers machined from Mycalex (McMaster Carr, Chicago, IL). Forty equally spaced BeCu rings are used to create a uniform field (typically, 5−12 V cm^{-1} in these studies) along the drift axis.

As ions reach the last ~1 cm of the drift tube (Figure 1) they leave the uniform field region and enter a high-pressure focusing field before being extracted into the differentially pumped OSC region. The high-pressure focusing element[42] consists of a stainless steel conical lens and a 0.20-cm-diameter BeCu exit orifice lens. The electrodes are separated by a Teflon isolator, and the assembly is mounted on the inside of the drift tube exit plate. The differentially pumped region extends from the exit plate of the drift tube to a skimmer cone that is positioned directly behind the drift tube exit orifice. The pressure in this region can be monitored by a capacitance manometer (model 640A Baratron from MKS, Andover, MA) and is on the order of 0.05 Torr (under the experimental conditions employed). The potential difference between the BeCu orifice plate and the skimmer cone defines the OSC voltage (V_{OSC}), which can be varied to induce fragmentation. No fragmentation is observed for $V_{OSC} < \sim 10$ in He.

Quadrupole Mass Filter, Octopole Collision Cell, and TOF Regions. Ions that exit the OSC region are focused into an Extrel quadrupole mass spectrometer. Typically, the pressure in this region during experiments is $\sim 10^{-5}$ Torr. The quadrupole can be operated to pass a selected m/z window over a ~20−4000 u range (or in transmission mode, as noted above). As ions exit the quadrupole they are decelerated to a desired kinetic energy and focused into the octopole collision cell. A stainless steel tube creates the collision cell body, and ions enter and exit the cell through electrically isolated end caps. Eight stainless steel rods are situated in three macor mounts that center the rods inside the collision cell body. Ports in the collision cell case allow target gases to be added to the cell and pressures (controlled by a Granville Phillips model 203 leak valve) to be monitored by a capacitance manometer (MKS model 640A Baratron). The pressure in the collision cell during CID experiments is typically maintained from ~1 to 4×10^{-4} Torr. In the studies presented below, a dc bias (−20 to −50 V) and rf potentials, opposite in phase for adjacent rods (2.2 MHz, 826.4 V_{pp}), are applied to the rods of the collision cell.

The primary ion beam can be transmitted through the source region [between a pulsing plate and an extraction grid (Ni mesh, Buckbee-Mears, 90% transmittance)] of the TOF and focused onto an on-axis collision dynode/dual-microchannel plate (MCP, Burle, Sturbridge, MA) detector. Several different experiments can be performed utilizing this detector and will be described in more detail below.

The orthogonal TOF mass spectrometer can be activated by applying 0.5−3.0-μs high-frequency (10^4 Hz), high-voltage (+500 to +2500 V) pulses (pulser model GRX-3.OK-H, Directed Energy Inc.) to the back plate of a two-stage TOF source. The final source grid establishes the flight tube potential (7000 V in most experi-

(36) Henderson, S. C.; Valentine, S. J.; Counterman, A. E.; Clemmer, D. E. *Anal. Chem.* **1999**, *71*, 291.
(37) Liu, Y.; Clemmer, D. E. *Anal. Chem.* **1997**, *69*, 2504.
(38) Hoaglund, C. S.; Valentine, S. J.; Clemmer, D. E. *Anal. Chem.* **1997**, *69*, 4156.
(39) Measurements of drift times as a function of injection voltage show that under the present experimental conditions, this heating/cooling process must be largely complete during the first few millimeters of the drift tube.
(40) Jarrold, M. F.; Honea, E. C. *J. Phys. Chem.* **1991**, *95*, 9181.
(41) Previous studies[19] of bradykinin indicate that at high injection energies, the doubly charged $[M + 2H]^{2+}$ are converted to $[M + H]^+$ via an endothermic proton-transfer process that forms HeH^+. The proton affinity of He is 42.5 kcal mol^{-1} (see: Lias, S. G.; Liebman, J. F.; Levin, R. D. *J. Phys. Chem. Ref. Data* **1984**, *13*, 695).
(42) This focusing element is similar in design to one used by Bowers, Weis, and co-workers (Kemper, P., personal communication).

ments) and defines a 17.5-cm-long field-free region. An electrostatic mirror at the back of the flight tube is generated by applying a uniform retarding potential field to 20 stainless steel rings. Reflected ions are detected by a pair of MCPs.

Acquisition of Ion Mobility/Time-of-Flight Data. It is useful to discuss peaks in the two-dimensional datasets using the "drift-(flight)" time (or $t_D(t_F)$) nomenclature we described previously.[19] Unless otherwise stated, values of $t_D(t_F)$ are reported as ms(μs). The data acquisition system has been described in detail elsewhere.[19] Briefly, an initial injection pulse activates a programmable delay generator (PDG) which is used to trigger pulses in the source region of the TOF instrument. In the present experiments, 256 windows (each $\sim$50 μs in duration) are used for the ion mobility separation. Flight times in the mass spectrometer are recorded using a time-to-digital converter (TDC) that is also initiated by the PDG pulse sequence. The TDC records the time that it takes for ions to reach the detector and can store up to 128 events for each TOF pulse sequence. The instrumental electronics and data acquisition system, including the initial injection pulse, PDG pulse sequence, TDC, and high-voltage TOF pulser are synchronized by an interface and controlled by a Pentium computer.

Determination of Mobilities, Collision Cross Sections, Drift Tube Resolving Power, and Calibration of *m*/*z*. It is useful to derive mobilities and collision cross sections from the nested datasets. The reduced mobilities of ions in a uniform field are obtained from[4]

$$K_0 = \frac{L}{t_D E}\frac{P}{760}\frac{273.2}{T} \quad (1)$$

where L is the drift tube length, P is the buffer gas pressure, t_D is the measured drift time, E is the electric field strength, and T is the buffer gas temperature. Experimental collision cross sections are derived from[43]

$$\Omega = \frac{(18\pi)^{1/2}}{16}\frac{ze}{(k_b T)^{1/2}}\left[\frac{1}{m_I}+\frac{1}{m_B}\right]^{1/2}\frac{t_D E}{L}\frac{760}{P}\frac{T}{273.2}\frac{1}{N} \quad (2)$$

where ze, N, k_b, m_I, and m_B correspond to the ion's charge, the neutral number density, Boltzmann's constant, the mass of the ion, and the mass of the buffer gas, respectively.

In the present experiments, the arrival time of ions at the detector, $t_{arrival}$, includes the time required for ions to drift through the mobility instrument and travel through the interface between the drift tube and the TOF mass spectrometer, as well as the time required for ions to travel through the TOF instrument (t_F). To determine the drift time (t_D) we correct the measured arrival time by

$$t_D = t_{arrival} - (t_C + t_{OSC} + t_F) \quad (3)$$

where t_C is the ion flight time through the evacuated drift tube and the region between the drift tube exit skimmer cone and the TOF source, t_{OSC} is the time spent in the OSC region, and t_F is the ion flight time in the TOF instrument. For CID studies in the octopole collision cell, the time required to travel between the drift and TOF regions depends on experimental parameters, such as the collision energy and buffer gas pressures. The corrections required at high collision cell pressures ($= 5 \times 10^{-4}$ Torr) can be substantial and are determined empirically; we generally do not attempt to determine mobilities from measurements where substantial corrections are required.

The OSC region also complicates mobility determinations. Ions exit the uniform field region of the drift tube and experience a poorly defined focusing field (which is usually tuned to increase ion transmission or influence fragmentation patterns). Under most conditions, we find that the measured drift times are dominated by the time spent in the uniform field of the drift tube. In this case, a multipoint calibration to a system with known mobilities can be used to correct the drift times. Under some OSC conditions (especially low extraction fields), peaks in the ion mobility distribution become substantially broader than expected. Increasing the extraction field created by the conical lens and BeCu orifice plate usually alleviates this problem. All of the other experimental parameters, E, L, P, and T, are precisely known such that the reproducibility of the measurement is excellent. Any two measurements normally agree to within $\sim$1.5%.

The resolving power $t_D/\Delta t$ (where Δt is defined as the full width at half-maximum (fwhm) of the ion mobility peak) for peaks in the injected-ion drift tube ranges from $\sim$20 to 25 (for singly charged ions) to as high as 60 for some multiply charged ions. Flight times (in the TOF instrument) are converted to m/z values using a standard multipoint calibration. The resolution ($m/\Delta m$ where Δm is the fwhm of the peak) of peaks in the TOF instrument ranges from 600 to 1300. The mass accuracy for parent ions is typically 50−100 ppm.

Sample Preparation and Ion Formation. Data shown for a model five-peptide component mixture containing Met-enkephalin (YGGFM, 98% purity, Sigma), Leu-enkephalin (YGGFL, 98% purity, Sigma), angiotensin II (NRVYIHPF, 98% purity, Sigma), angiotensin I (NRVYIHPFHL, 98% purity, Sigma), and substance P (RPKPQQFFGLM, 98% purity, Sigma) were obtained using nanoelectrospray ionization. Here, a solution containing 10 μg mL^{-1} of the five-peptide component mixture (2 μg mL^{-1} of each peptide) in 98:2 (% volume) water/acetic acid was directly infused through the nanoelectrospray ion source.[44] A microelectrode holder (World Precision Instruments, Sarasota, FL) was positioned using an x, y, z position manipulator. The original silver wire of the microelectrode holder was replaced with a stainless steel wire (45-mm length, 0.1-mm i.d.), which was then inserted into a borosilicate glass capillary (1.5-mm o.d., 0.86-mm i.d.) containing several microliters of sample solution. Needle stability was ensured by tightening the connector on the microelectrode holder. The glass capillary was pulled ($\sim$5 μm) using a Sutter Instrument Company (Novato, CA) P-97 Flaming/Brown micropipet puller,[45] and the sample was loaded into the capillary using a 0.56-mm-diameter stainless steel syringe. The nanoelectrospray needle voltage was optimized between 1.0 and 1.6 kV.

(43) Mason, E. A.; McDaniel, E. W. *Transport Properties of Ions in Gases*; Wiley: New York, 1998.

(44) Wilm, M.; Mann, M. *Anal. Chem.* **1996**, *68*, 1.. Cargile, B. J.; McLuckey, S. A.; Stephenson, J. L. *Anal. Chem.* **2001**, *79*, 1277.

(45) The parameter set for a two-step pulling procedure on the P-97 capillary puller from Sutter is as follows: heat 620, pull strength 0, velocity 50, cooling time 150, repeat.

Solutions containing 1.0 mg mL^{-1} of the lyophilized tryptic peptide mixture,[46] 0.25 mg mL^{-1} substance P, or 0.5 mg mL^{-1} (0.25 mg mL^{-1} of each component) of angiotensin I and angiotensin III (RVYIHPF, 98% purity, Sigma) were ionized using a conventional electrospray source. Solution flow rates of 0.08 mL hr^{-1} were controlled by a syringe pump (kd Scientific, New Hope, PA). The ESI voltage used was −3800 V.

RESULTS AND DISCUSSION

Overview. The results and discussion presented below are intended to illustrate the utility of several instrumental configurations for the analysis of complex peptide mixtures. We begin with an example that describes the analysis of a five-component peptide mixture. This well-defined sample allows us to examine the detection limits of the current mobility-TOF configuration as well as detection limits associated with parallel collisional activation studies. We subsequently describe two examples that utilize a configuration that allows 2° fragments to be examined. As discussed above, although the drift times of 1° fragments (created in the OSC region) are coincident with the parent ion drift times, m/z ratios of the 1° fragments are virtually independent of the parent ion mass. The exception to this is when the m/z of a 1° fragment is the same as the value of its parent. By generating and examining 1° fragments, it is possible to circumvent limitations that arise from the fact that the mobilities and m/z ratios of parent ions are correlated. Finally, we present an analysis of a tryptic digest of β-casein. The two-dimensional $t_D(t_F)$ dataset for this system exhibits a complicated distribution of peaks. Collisional activation of the complete mixture of parent ions results in a complex pattern of 1° fragments. We examine this dataset in order to explore the utility of these patterns for peptide identification.

Analysis of a Mixture of Five Peptides: Drift(Flight) Time Distributions and Parallel CID. Nested distributions for electrosprayed peptide mixtures containing five components (substance P, angiotensins I and II, Met-enkephalin, and Leu-enkephalin) are shown in Figure 2. The parent ion distribution is obtained by setting the quadrupole mass filter to transmit all ions and evacuating the collision cell. The nested dataset shows eight distinct peaks corresponding to $[M + H]^+$ ions for Met-enkephalin [4.08(22.49, m/z = 574.2)] and Leu-enkephalin [4.08(22.14, m/z = 556.3)], $[M + 2H]^{2+}$ ions of angiotensin I [3.66(23.89, m/z = 648.4)], angiotensin II [3.29(21.50, m/z = 523.3)], and substance P [3.82(24.36, m/z = 674.4)], and $[M + 3H]^{3+}$ ions of angiotensin I [2.87(19.58, m/z = 432.6)], angiotensin II [2.56(17.62, m/z = 349.2)], and substance P [2.66(19.95, m/z = 449.9)]. Information about the relative intensities of each peak can be obtained by examining the mass spectrum (also shown), obtained by integrating across all drift times.

Figure 2 also shows the distribution of peaks that is obtained upon adding 1.8×10^{-4} Torr of argon to the octopole collision cell. In addition to most of the features in the parent distribution, many a-, b-, y-type and immonium fragment ions, as well as ions that result from internal fragmentation, are observed.[47] Integration across narrow drift time ranges allows us to generate fragmentation data for individual parents. Examples of slices at drift times of 2.66, 2.87, and 4.08 ms that correspond to the $[M + 3H]^{3+}$ ions of substance P and angiotensin I and the $[M + H]^+$ ions of Met- and Leu-enkephalin are shown in Figure 2. It is straightforward to assign peaks in the fragmentation data for the $[M + 3H]^{3+}$ ions of substance P and angiotensin I because these ions have very different drift times (2.66 and 2.87, respectively). However, the $[M + H]^+$ peaks of Met- and Leu-enkephalin have similar drift times such that the fragment peaks are coincident with more than one parent. In fact, the sequences of Met- and Leu-enkephalin vary only in the C-terminal amino acid residue. Therefore, many of the N-terminal and internal fragments that have coincident drift times, including the b_4 (m/z = 424.9), a_4 (m/z = 397.2), b_3 (m/z = 278.2), GGF (m/z = 262.8), and GF (m/z = 205.6) fragment ions, may arise from one or both of these parent ions. Several fragments are unique to the individual parent; the m/z = 393.1 ion corresponds to the y_4 fragment ion of Leu-enkephalin; the m/z ratios = 354.1, 297.0, 149.8, and 104.3 peaks are assigned to the y_3, y_2, y_1, and M immonium fragments for Met-enkephalin, respectively.

Detection Limits of Drift(Flight) Time and Parallel Fragmentation Experiments. Numerous studies were carried out using solutions of known concentrations of commercially available peptides to assess detection limits. It is worthwhile to note that in this analysis, the observed peaks that are considered are present at levels that are well above the typical signal-to-noise (S/N) ratio of 3.0 used to define limits of detection. Thus, the values we report are actually upper limits to the lowest levels that would be detectable at S/N = 3. For parent ion drift(flight) time distributions, typical detection limits range from ∼5 to 50 fmols of consumed peptide, a marked improvement compared to the limits of ∼0.5−3.0 pmol reported previously for analysis of mixtures without CID.[36,38] The improvement arises from several instrumental changes we have made that increase transmission through the source and drift tube and improve the duty cycle of the TOF instrument.

Upon introduction of a collision gas for parallel fragmentation studies, we note that detection limits are somewhat higher, especially for fragments. The parent ion can still be observed at relatively low levels of consumed sample (<50 fmol). The most abundant fragment peaks, such as M, y_1, b_9^{2+}, a_{10}^{2+}, $b_{10} - NH_3^{2+}$, and b_{10}^{2+} of the $[M + 3H]^{3+}$ ion of substance P and the H, y_4^{2+}, b_9^{2+}, and b_5 ions of the $[M + 3H]^{3+}$ ions of angiotensin I, are clearly observed before consumption of ∼100 fmol of sample. In some experiments, these levels are even lower. As more sample is consumed, peaks associated with less abundant fragments become discernible. Overall, it appears that detection limits of fragments are correlated with the abundance of the remaining parent ion peak; that is, there is no evidence for substantial loss of parents or fragments in the collision cell. Thus, we have estimated limits of detection for all of the fragments observed in Figure 2. This estimate comes from combining information about the amount of consumed sample in the very short time scale

(46) The β-casein digest was prepared by combining a 20 mg mL^{-1} solution of β-casein (Sigma, 90%) in 0.2 M ammonium bicarbonate (EM Science) with a 0.2 mg mL^{-1} trypsin (Sigma, bovine) solution in 0.2 M ammonium bicarbonate with an ∼50-fold excess protein by weight and incubating for 20 h at 37° C. The trypsin was filtered from the digest using a microconcentrator (microcon 10, Amicon), and the peptides that remained were lyophilized.

(47) Assignments were made by comparison of experimental m/z ratios with values from the MSProduct program from Protein Prospector http://prospector.ucsf.edu. Fragment nomenclature is consistent with that described by: Biemann, K. *Biomed. Environ. Mass Spectrom.* **1988**, *16*, 99. Biemann, K. *Method Enzymol.* **1990**, *193*, 886.

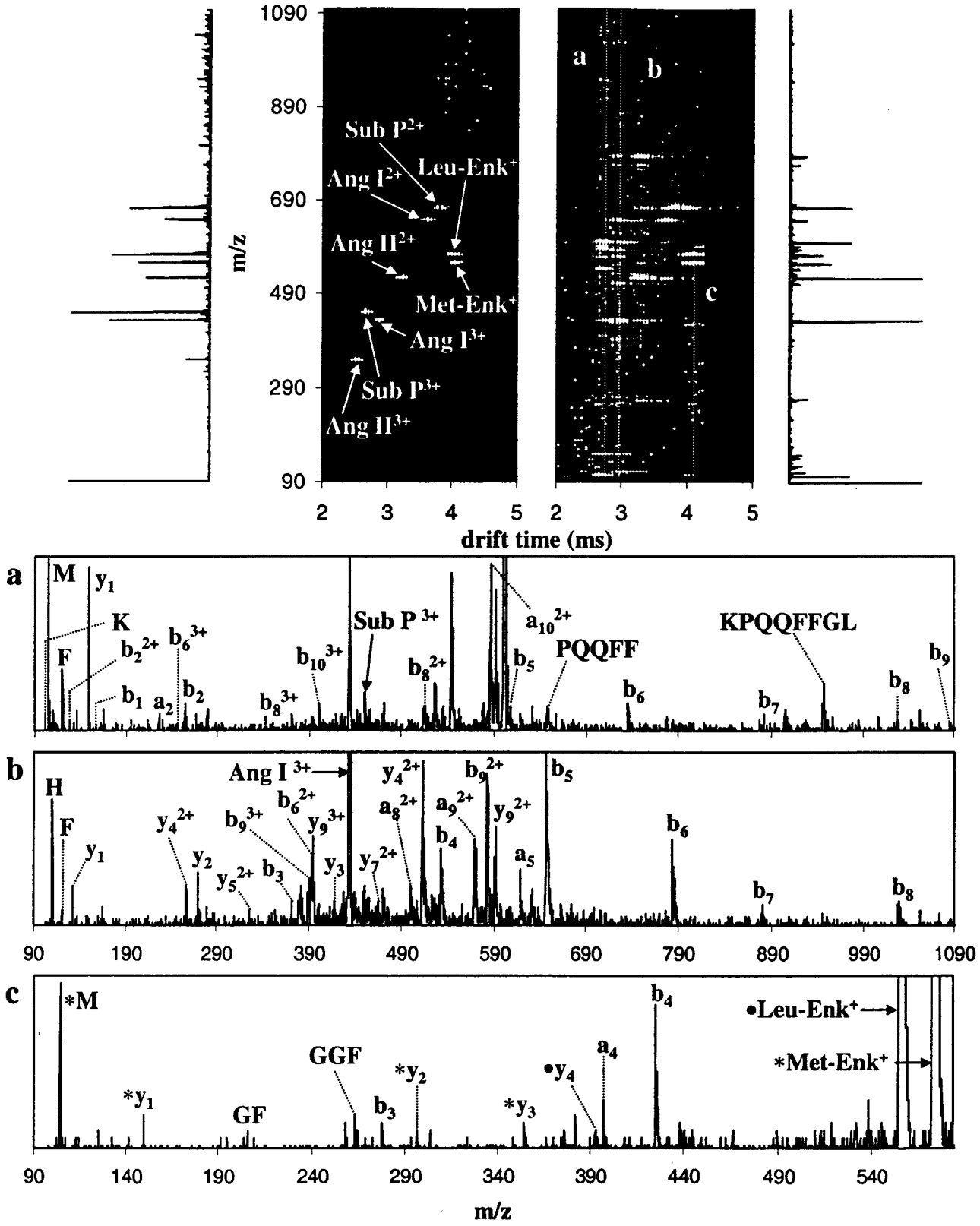

Figure 2. (Top) Nested distributions and integrated mass spectra for an electrosprayed mixture of Met-enkephalin, Leu-enkephalin, angiotensin II, angiotensin I, and substance P. The distribution on the left was obtained using helium buffer gas and $V_{OSC} = 5$. The distribution on the right was obtained after adding 1.8×10^{-4} Torr argon to the octopole collision cell. Mass spectral slices of the data can be obtained by integrating over small drift time ranges. (Bottom) The fragmentation spectra obtained at drift times centered at 2.66, 2.87, and 4.08 ms (indicated by the dotted lines in the top right distribution) are shown for $[M + 3H]^{3+}$ parent ions of substance P (a) and angiotensin I (b) and the $[M + H]^{+}$ parent ions of both Met- and Leu-enkephalin (c). Asterisks (*) and solid circles (●) in peak labels from spectrum c correspond to fragments that could arise from Met- and Leu-enkephalin parent ions, respectively. Peak labels without symbols represent assignments that could correspond to both parents. These data were obtained using helium buffer gas. See text for details.

Table 1. Detection Limits for Peptides and Associated Fragments upon Parallel CID

parent ion	DL[a] (fmol)	t_D (ms)	assigned fragments[b] (est DL)[c]
[Met-enkephalin + H]$^+$	17	4.08	M(380), y_1(1500), GF(4600), GGF(3000), b_3(3600), y_2(2300), y_3(1800), a_4(2300), b_4(870)
[Leu-enkephalin + H]$^+$	17	4.08	GF(4600), GGF(3000), b_3(3600), a_4(2300), b_4(870), y_4(2300)
[substance P + 2H]$^{2+}$	3	3.82	M(120), y_1(550), y_2(350), a_8^{2+}(650), b_{10}^{2+}(430), b_9(550)
[angiotensin I + 2H]$^{2+}$	3	3.66	H(390), y_1(650), VY(220), a_6^{2+}(650), HPF/PFH(480), a_5(650), b_6(230)
[angiotensin II + 2H]$^{2+}$	6	3.29	H(58),F(550),y_2(130),y_3(550),y_4(180), a_5(220),a_6(280),b_6(46)
[substance P + 3 H]$^{3+}$	4	2.66	K(480), M(15), F(160), b_2^{2+}(650), y_1(63), b_1(770), a_2/a_4^{2+}(480), b_6^{3+}(770), b_2(320), b_8^{3+}(550), b_{10}^{3+}(320), b_8^{2+}(350), b_9^{2+}(66), a_{10}^{2+}(62), $b_{10}-NH_3^{2+}$(73), b_{10}^{2+}(11), b_5(350), PQQFF(350), b_6(320), b_7(650), KPQQFFGL(200), b_8(650), PKPQQFFGL(650), b_9(770)
[angiotensin I + 3 H]$^{3+}$	5	2.87	H(88), F(550), y_1(260), y_4^{2+}(260), y_2(190), y_5^{2+}(550), b_3(390), HPF/PFH(260), b_9^{3+}(200), b_6^{2+}(160), y_9^{3+}(120), y_3(390), y_7^{2+}(480), a_8^{2+}(260), y_4^{2+}(68), b_4(140), a_9^{2+}(120), b_9^{2+}(73), y_9^{2+}(110), a_5(180), IHPFH(280), b_5(47), b_6(130), b_7(430), b_8(390)
[angiotensin II +3 H]$^{3+}$	3	2.56	F(160), b_2^{2+}(350), a_4^{2+}(390), b_4^{2+}(550), a_3(550), b_3(650), y_3(430), y_4(350)

[a] Detection limits for parent ions were determined by a series of studies carried out using different solution concentrations. Values correspond to the amount of consumed sample that is required to produce S/N = 3. See text for discussion. [b] Fragment assignments are consistent with ref 47. [c] Detection limits for fragment ions are given in fmols and estimated using DL = peak intensity (at S/N = 3) × total amount consumed (per peptide component)/peak intensity.

detection limit studies (~30 s) with the peak abundance measured in longer time studies. Table 1 provides a summary of these estimates. Values range from as low as ~20 fmol (for the M immonium ion from substance P) to as high as ~4.6 pmols for less abundant fragments.

Mobility and *m*/*z* Selection and Dissociation of 1° Fragments. We have explored several experimental conditions for generating and selecting 1° fragment ions for a number of peptides, proteins, and several types of mixtures. Figure 3 shows several $t_D(t_F)$ datasets recorded for substance P. At low OSC potential (5 V) and no collision gas, single narrow peaks at 2.77-(19.95, m/z = 449.9) and 4.19(28.07, m/z = 898.8) correspond to the $[M + 3H]^{3+}$ and $[M_2 + 3H]^{3+}$ ions, respectively. Other peaks in the distribution show somewhat more complicated behavior. The $[M + 2H]^{2+}$ ion exhibits two peak maxima at 3.87(24.36, m/z = 674.4) and 3.45(24.36, m/z = 674.4) (although not completely apparent from the two-dimensional dataset) that correspond to two different conformations of this ion. The ion mobility distribution for the m/z = 1347.7 ion shows a broad feature that extends from 3.9 to 5.5 ms and two smaller features at 5.93 and 7.03 ms. We have previously used combined molecular dynamics and collision cross section calculations to assign analogous peaks in several systems;[48] here, we assign these features to the $[M + H]^+$ monomer (7.03 ms), the $[M_2 + 2H]^{2+}$ dimer (5.93 ms), and a distribution of unresolved multiply charged multimers having the general formula $[M_n + nH]^{n+}$ (from 3.9 to 5.5). There is no evidence for fragment ion formation under these conditions.

Figure 3 also shows a distribution that was obtained upon increasing the OSC potential to 29.3 V. Several peaks show low levels of fragmentation; however, a substantial fraction of the $[M + 3H]^{3+}$ ions dissociate. A mass spectral slice taken at 2.77 ms shows that under these conditions, dissociation of the $[M + 3H]^{3+}$ ion primarily gives rise to a peak at m/z = 444.4 that corresponds to a loss of water (b_{11}^{3+}) and a peak at m/z = 600.4 that corresponds to the b_{10}^{2+} fragment.[49]

The final nested dataset in Figure 3 shows a selected-fragment ion distribution for the b_{10}^{2+} ion that was formed by collisional activation in the OSC region using V_{OSC} = 29.3. Here, we have fixed the quadrupole to transmit m/z = 600.4 and introduced 1.8 × 10^{-4} Torr of argon into the octopole collision cell. In this case, large features at 2.77 ms associated with peaks that we assigned to the $[M + 3H]^{3+}$ and b_{11}^{3+} ions are absent; they have been removed by the quadrupole mass filter. Instead, a new series of peaks is observed at 2.77 ms; these correspond to 2° fragments that arise from dissociation of the 1° b_{10}^{2+} fragment. The 2° fragment ions have drift times that are coincident with the drift time of the $[M + 3H]^{3+}$ parent ion. A slice across the distribution of peaks that is formed upon activation in the octopole shows that series of a- and b-type fragments are present. Many of the fragments that are not labeled in this spectrum correspond to internal sequence fragments as well as fragments that arise due to loss of small neutral molecules (i.e., H_2O, NH_3).

An important factor associated with subsequent activation of 1° fragments can be understood by considering the location of the b_{10}^{2+} peak in the data in Figure 3. This peak arises from dissociation of the high-mobility $[M + 3H]^{3+}$ parent. Because the fragment m/z ratio is established after the mobility separation, drift and flight times are no longer strongly correlated, as is the case for $[M + H]^+$ and $[M + 2H]^{2+}$ parent ions (see the dashed lines in Figure 3). Thus, many 1° fragment ions are effectively spread out across the $t_D(t_F)$ distribution. This has the effect of increasing the peak capacity and also simplifies m/z selection in the quadrupole.

Mobility/(*m*/*z*) Selection and Dissociation of 1° Fragments That Arise from Different Parent Ions. An additional example that involves the selection of primary fragment ions is shown in Figure 4 for a mixture of angiotensin III and angiotensin I. This example illustrates a case in which the combination of mobility separation and 2° ion formation provides assignment of an ion that was initially unexpected. The sequences of angiotensin III and I (RVY*IHPF* and NR*VYIHPFHL*) contain three four-residue fragments having a mass of 512.3, the portion of the sequences shown in italics as well as the italic/underlined portion. We

(48) Counterman, A. E.; Valentine, S. J.; Srebalus, C. A.; Henderson, S. C.; Hoaglund, C. S.; Clemmer, D. E. *J. Am. Soc. Mass Spectrom.* **1998**, *9*, 743.

(49) We note that the buffer gas used for experiments can have a significant effect on the amount of fragmentation observed. More efficient fragmentation occurs when using argon, as compared to helium, for the drift tube buffer gas. This is rationalized on the basis of the difference in the center-of-mass collision energy available from collisions with argon versus helium.

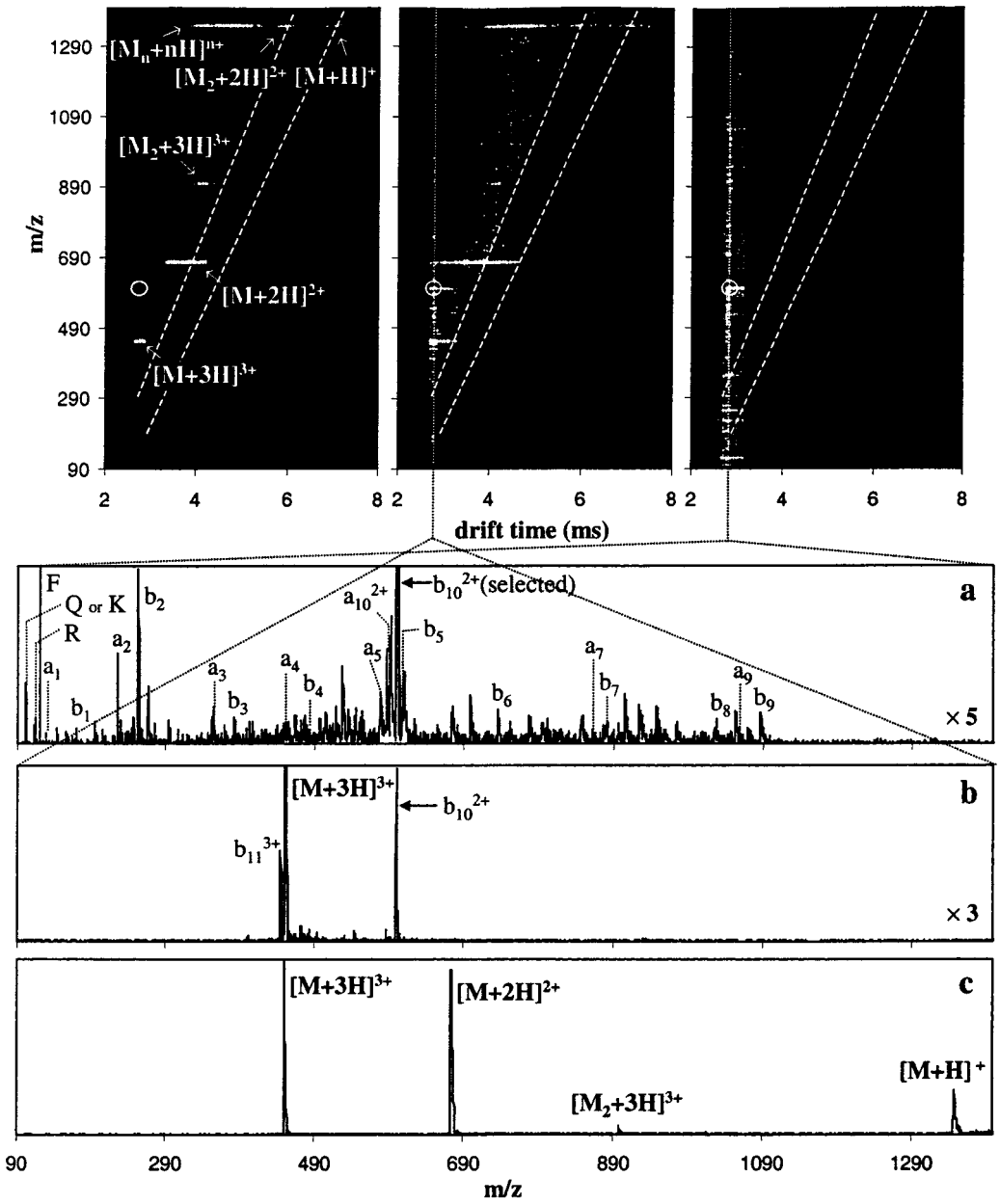

Figure 3. (Top) Nested distributions for electrosprayed substance P ions. The distribution on the left was obtained using $V_{OSC} = 5$ (only parent ions are observed). The dotted lines provide visual guides that indicate the locations of the $[M + H]^+$ and $[M + 2H]^{2+}$ charge state families typically observed in nested datasets. The distribution in the center was obtained by setting $V_{OSC} = 30$ to induce fragmentation. The distribution on the right was also recorded using $V_{OSC} = 30$. Here, the quadrupole was set to select $m/z = 600.4$ (b_{10}^{2+}), and 1.8×10^{-4} Torr argon was added to the octopole collision cell. The circle indicates the position of the b_{10}^{2+} fragment. (Bottom) Mass spectral slice a is centered around a drift time (2.77 ms) coincident with the $[M + 3H]^{3+}$ ion (indicated at the top by the vertical dotted line) and shows the 2° fragmentation pattern for the selected 1° b_{10}^{2+} fragment. Mass spectral slice b, obtained in a fashion similar to (a), shows the distribution prior to quadrupole selection of the 1° b_{10}^{2+} fragment ion. Spectrum c is obtained by integrating the two-dimensional dataset (top left) over all drift times. These data were obtained using helium buffer gas. See text for details.

expected to see a y_4 fragment ion for each of these parents at $m/z = 513.3$. The data in Figure 4 indicate different behavior. At a low OSC potential of 5.0 V, we observe features at 3.71(16.64, $m/z = 311.2$) and 4.29(19.57, $m/z = 432.6$), 4.56(20.30, $m/z = 466.3$) and 5.24(23.89, $m/z = 648.4$), and 7.82(28.54, $m/z = 932.1$) and 9.46(33.62, $m/z = 1295.7$) that correspond to the $[M + 3H]^{3+}$, $[M + 2H]^{2+}$, and $[M + H]^+$ ions of angiotensin III and angiotensin I, respectively. As discussed above, the broad features at drift time ranges of 4.9−6.6 (angiotensin III) and 5.0−6.9 (angiotensin I) correspond to multiply charged multimers. The parent ion distribution also exhibits low levels of fragmentation under the conditions employed. Note that argon was used as the buffer gas in these studies. Upon increasing the OSC potential to 16.2 V, abundant 1° fragment peaks (including peaks at $m/z = 513.3$) are observed. The very different drift times of the $[M + 3H]^{3+}$ ions of angiotensin III and angiotensin I (3.71 and 4.29 ms, respectively), allow the 1° fragments to be assigned to a specific parent.

When the quadrupole is set to transmit $m/z = 513$ and 1.9×10^{-4} Torr of argon is added to the octopole collision cell, the 1°

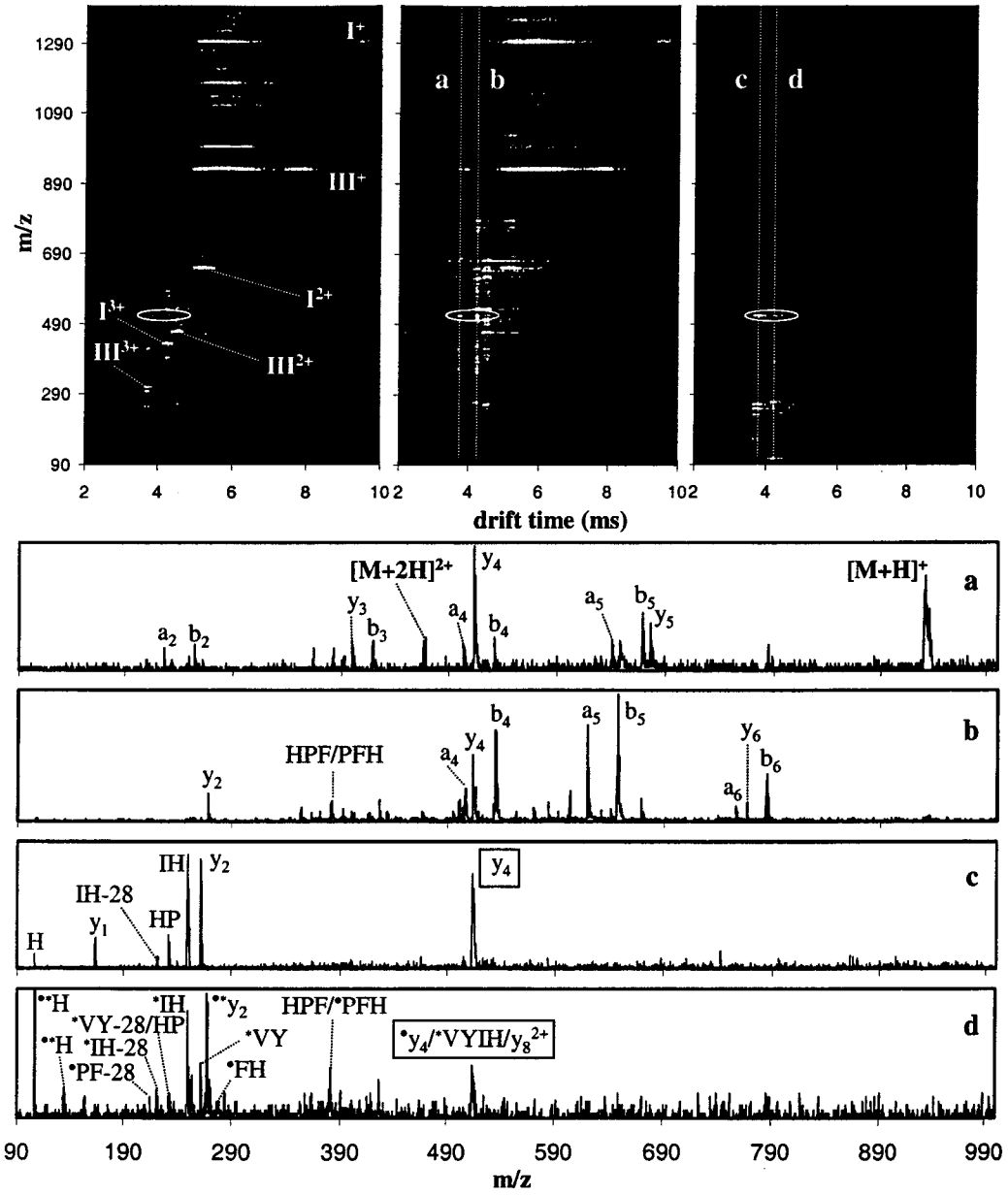

Figure 4. (Top) Nested distributions for an electrosprayed mixture of angiotensin III and angiotensin I. The distribution on the left was obtained using $V_{OSC} = 5$. The distributions in the center and on the right were obtained using $V_{OSC} = 16.2$. The distribution on the right was obtained after adding 1.9×10^{-4} Torr argon to the octopole collision cell. The dotted lines delineate the center of the drift time integration region used to obtain the mass spectral slices shown at the bottom. Circles indicate the location of 1° fragments at $m/z = 513$. (Bottom) Spectra a ($t_D = 3.71$ ms) and b ($t_D = 4.29$ ms) correspond to the fragmentation patterns obtained for the $[M + 3H]^{3+}$ ions of angiotensin III and angiotensin I, respectively. Spectra c ($t_D = 3.71$ ms) and d ($t_D = 4.29$ ms) correspond to the 2° fragmentation patterns for the selected 1° fragment ions (at $m/z = 513$) of these parents. Peak labels in spectrum d include symbols that represent possible origins of the assigned 2° fragments. Asterisks (*) correspond to 2° fragments that could arise from the 1° y_4 fragment, solid circles (●) correspond to 2° fragments that could arise from the 1° VYIH fragment, and all of the peaks could correspond to the 1° y_8^{2+} fragment. These data were obtained using argon buffer gas. See text for details.

fragments yield different distributions of 2° fragments. The corresponding mass spectral slices at 3.71 and 4.29 ms (coincident to the $[M + 3H]^{3+}$ parent ions of angiotensin III and I) are also shown. Secondary fragment peaks from CID of the 1° y_4 ion of angiotensin III $[M + 3H]^{3+}$ at $m/z = 263.1$, 251.2, 235.1, 223.2, 166.1, and 110.1 are assigned to the y_2, IH, HP, IH-28, y_1, and H immonium fragments, respectively. The mass spectral slice taken at 4.29 ms (for angiotensin I) also shows evidence for fragmentation of the 1° y_4 ion. Peaks at $m/z = 382.2$, 285.1, 269.2, 217.1, 138.0, and 110.1 could correspond to the 2° fragments from the 1° y_4 fragment. However, additional peaks are observed at $m/z =$ 263.1, 251.2, 235.1, and 223.2 which cannot be due to the 1° y_4 fragmentation but could correspond to 2° fragments that are consistent with the VY, IH, HP, and IH-28 ions from fragmentation of the 1° VYIH internal fragment. The 1° y_8^{2+} fragment could give rise to all of the observed 2° fragment peaks for angiotensin I. Thus, we cannot rule out the possibility that these 2° fragments arise from both the 1° y_4 and VYIH fragments or the 1° y_8^{2+} fragment (or a combination of both).

The ability of the combined mobility separation and m/z selection to distinguish between fragmentation patterns for isobaric ions should be useful in the analysis of systems in which

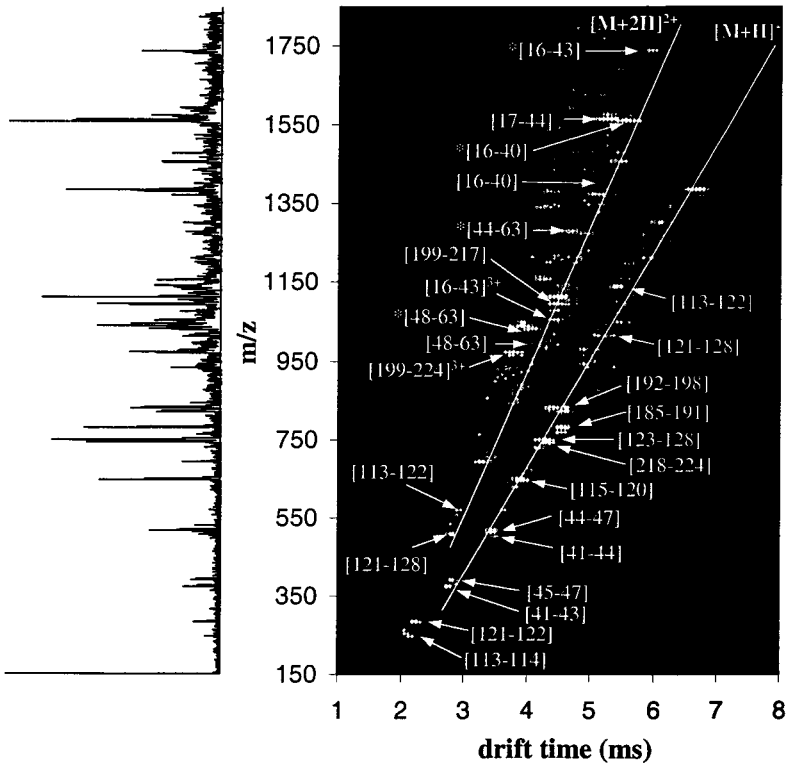

Figure 5. Nested distribution for an electrosprayed mixture of tryptic peptides of β-casein. Peak labels correspond to sequence positions within the protein that are in agreement with the experimental results expected from the tryptic digestion. Asterisks (*) correspond to peptides that are phosphorylated at serine residues. The solid lines provide visual guides corresponding to the $[M + H]^+$ and $[M + 2H]^{2+}$ charge state families. The mass spectrum shown on the left is obtained by integrating the two-dimensional data over all drift times. These data were obtained using helium buffer gas. See text for details.

isomeric species are present (e.g., combinatorial libraries of peptides).

Parallel CID of a Large Mixture, Tryptic Peptides of β-Casein. Figure 5 shows a two-dimensional nested distribution for a mixture of tryptic peptides obtained from β-casein (a 209-residue protein with a molecular weight of ~23.5 kDa). Most peaks fall into families corresponding to $[M + H]^+$ and $[M + 2H]^{2+}$ ions; some higher charge state ions ($[M + 3H]^{3+}$ and $[M + 4H]^{4+}$) are also observed. Often, higher charge states can be assigned to fragments that arise from incomplete digestion. From comparisons of experimental m/z values with calculated values for expected tryptic peptides,[50] we assign 13 peaks in the $[M + H]^+$ family, 10 peaks in the $[M + 2H]^{2+}$ family, and 2 peaks to $[M + 3H]^{3+}$ ions (11 of 14 of the expected fragments). Additionally, we observe 9 peaks that can be assigned to peptides that arise from incomplete digestion: $[M + H]^+$ ions of INKK, KIEK, HKEMPFPK, and VKEAMAPKHK; and $[M + 2H]^{2+}$ ions of HKEMPFPK, VKEAMAPKHK, KIEKFQsEEQQQTEDELQDK (where s corresponds to phosphorylated serine residues in the sequence), RELEELNVPGEIVESLSSSEESITR, and ELEELNVPGEIVESLSSSEESITRINKK. Four peptides are phosphorylated, FQsEEQQQTEDELQDK [4.01(40.40, m/z = 1032.0], KIEKFQsEEQQQTEDELQDK [4.71(44.95, m/z = 1280.6)], RELEELNVPGEIVEsLsssEESITR [5.53(49.56, m/z = 1560.7], and RELEELNVPGEIVEsLsssEESITRINK [5.94(52.28, m/z = 1738.7]. Several peaks cannot be assigned to expected tryptic fragments, peptides generated from incomplete digestion or chymotryptic activity, or expected posttranslationally modified tryptic fragments.

Figure 6 shows a two-dimensional nested dataset obtained when 2.5×10^{-4} Torr of argon gas is added to the octopole collision cell. In addition to most of the features that were apparent in Figure 5, many new peaks corresponding to fragment ions are observed. Under the conditions used to record these data, fragmentation of both $[M + H]^+$ and $[M + 2H]^{2+}$ ions is apparent.

The origin of many fragments can be deduced by examining mass spectral slices over narrow drift time ranges. Figure 7 shows example plots of such data. The slice centered at $t_D = 4.48$ shows a mass spectrum that includes the $[VLPVPQK + H]^+$ [4.54(35.18, m/z = 780.8)] and $[AVPYPQR + H]^+$ [4.42(36.28, m/z = 830.2)] parent ions. Although the two parent ions are not entirely resolved, based on differences in drift times, it is possible to assign the peaks to fragments that are expected for CID of both parent sequences. Many other fragment assignments are not unambiguous. That is, peaks could correspond to more than one peptide that is present in the drift time slice. For example, the fragment peak at 4.60(30.06, m/z = 568.1) could correspond to the y_5 (m/z = 568.4) fragment of $[VLPVPQK + H]^+$ or the $VPYPQ - NH_3$ (m/z = 568.3) fragment of $[AVPYPQR + H]^+$. We note that although not all fragments can be unambiguously assigned, the approach allows much more progress than could be made by examining the fragmentation spectrum of the complete mixture.

(50) Assignments were made by comparison of experimental m/z ratios with values generated from the PeptideMass program (Wilkins, M. R.; Lindskog, I.; Gasteiger, E.; Bairoch, A.; Sanchez, J.-C.; Hochstrasser, D. F.; Appel, R. D. *Electrophoresis* **1997**, 18, 403.) on the ExPASy Molecular Biology Server http://ca.expasy.org/.

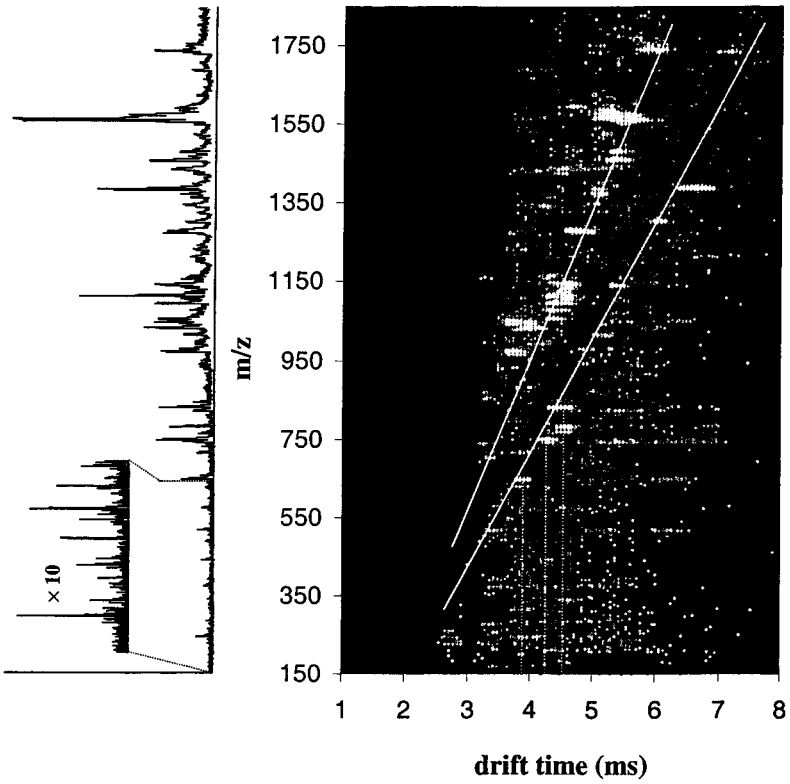

Figure 6. Nested distribution for the same β-casein tryptic mixture as in Figure 5 after 2.5×10^{-4} Torr of argon was added to the octopole collision cell. The solid lines provide visual guides corresponding to the $[M + H]^+$ and $[M + 2H]^{2+}$ charge state families. The mass spectrum shown on the left is obtained by integrating the two-dimensional data over all drift times. The dotted lines represent the center of the drift time integration regions used to obtain the mass spectral slices in Figure 7. These data were obtained using helium buffer gas. See text for details.

Several other representative slices are also shown in Figure 7. The mass spectrum centered at $t_D = 4.30$ ms shows fragmentation patterns for the $[EMPFPK + H]^+$ [4.30(34.45, $m/z = 748.8$)] and $[GPFPIIV + H]^+$ [4.30(34.32, $m/z = 742.5$)] parents. Here, 21 fragment peaks can be assigned unambiguously, 9 to the $[EMPFPK + H]^+$ parent ion and 12 to the $[GPFPIIV + H]^+$ parent ion. The peak at $m/z = 245.2$ corresponds to expected internal b-type peptide fragments FP and PF, which could arise from both of the parents. The final slice shown in Figure 7 contains only one parent, the $[EAMAPK + H]^+$ [3.89(32.04), $m/z = 646.0$] ion. These fragment peaks are straightforward to assign.

A complete analysis of the fragmentation dataset (Figure 7) has been carried out; however, a detailed discussion of the entire analysis is too extensive to present here. A brief summary is appropriate. It is possible to find at least a few (up to ~10) unique fragment ions of each of the expected tryptic fragments as well as many of the other parents (i.e., sequences that correspond to incomplete digestion and posttranslationally modified peptides). Most of the fragments appear to arise from dissociation of the $[M + 2H]^{2+}$ ions;[51] however, fragments from the $[M + H]^+$ parents are clearly present and provide valuable information. Many of the observed peaks occur at m/z ratios that are consistent with fragments from more than one parent that is present within the mass spectrum at a specific drift time, as illustrated in Figure 7.

Table 2 provides a summary of a limited number of slices that are representative of many other slices that have been analyzed. The information that is provided here is intended to give an idea about the fraction of ions that can be unambiguously assigned across various regions of the dataset. The complete analysis contains information about the fragmentation of ~20 parent ions. At short drift times, many of the small parent ions yield fragments that are nearly all unambiguously assigned.

Summary of Instrumental Capabilities. From the above discussion, it should be clear that the instrument in Figure 1 can be operated in a number of different ways. A flow diagram that summarizes the primary approaches that we commonly employ is shown in Figure 8. Here, we assume that experiments are initiated when a sample is electrosprayed into the instrument. We are in the process of incorporating several different condensed-phase separation methods at the front end of our instrument as a means of simplifying mixtures.[52] These approaches are not included in this summary.

In most cases, before experiments are initiated, it is useful to focus the distribution of electrosprayed ions into various regions of the instrument and examine the response of each region. This is essentially a diagnostic procedure that ensures that we are not discriminating against ions at any point in the instrument. The process usually begins by disabling the ion trap and focusing a beam through the drift tube, quadrupole, collision cell, and TOF source regions until ions hit the on-axis detector. As illustrated in path a of the flow diagram, several types of experiments can be conducted prior to enabling the ion trap. For example, at low OSC potentials, the quadrupole can be scanned to obtain a mass

(51) Dissociation of different peptide ion charge states has been discussed by: Wysocki, V. H.; Tsaprailis, G.; Smith, L. L.; Breci, L. A. *J. Mass Spectrom.* **2000**, *35*, 1399.

(52) Clemmer, D. E.; Hoaglund-Hyzer, C. S.; Srebalus-Barnes C. A. Work in progress.

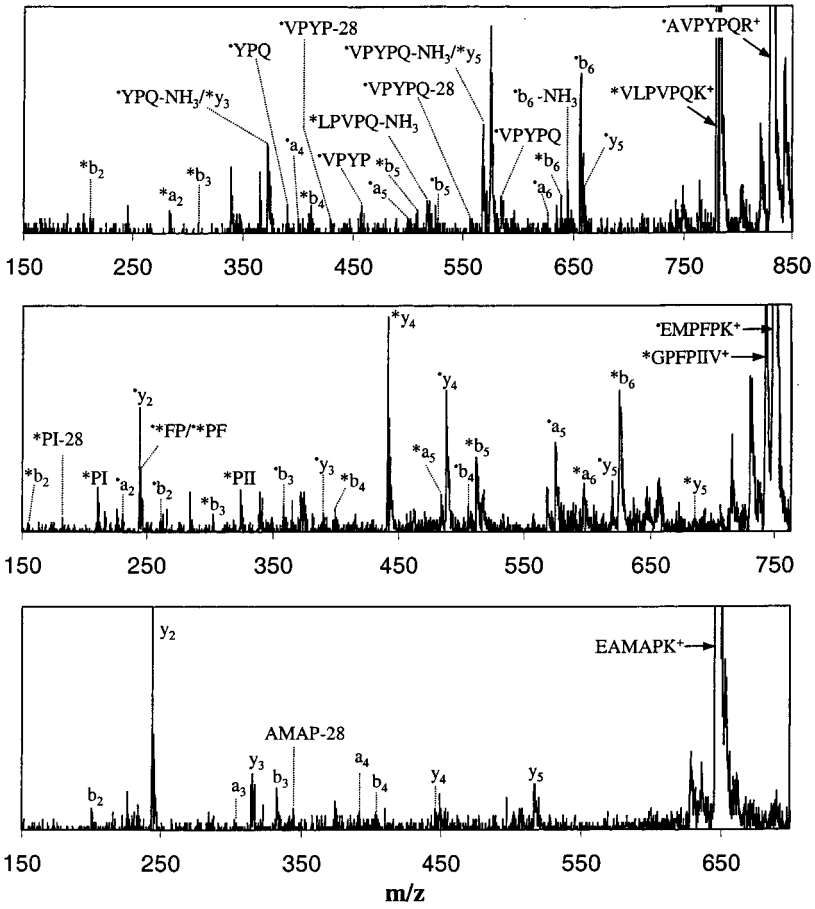

Figure 7. Mass spectral slices taken from the data shown in Figure 6. The top spectrum shows the fragmentation patterns for $[VLPVPQK + H]^+$ (∗) and $[AVPYPQR + H]^+$ (●) parent ions. The middle spectrum shows the fragmentation patterns for $[GPFPIIV + H]^+$ (*) and $[EMPFPK + H]^+$ (●) parent ions. The bottom spectrum corresponds to the fragmentation pattern arising from dissociation of the $[EAMAPK + H]^+$ parent ion. Asterisks (*) and solid circles (●) are included in the peak labels to indicate the parent ion of origin for each fragment. Labels without a symbol represent assignments for fragments that could correspond to both parent ions. See text for details.

spectrum of the distribution of ions from the source. Scanning the quadrupole at high OSC potentials provides information about parents and fragments that are formed.

Substantially more capabilities come about from enabling the TOF region (pathway b of Figure 8). In this case, the capabilities are similar to those that are found in ESI-Q-TOF instruments.[53] That is, at low OSC voltages, the quadrupole can be set to transmit all ions and the TOF region is used to record the distribution of ions from the source. Upon enabling the quadrupole and introducing a collision gas into the octopole collision cell, it is possible to carry out MS/MS studies. Finally, it is possible to increase the OSC voltage to generate 1° fragments for additional MS/MS studies. In this case, the OSC region of the drift tube is used in a fashion similar to the capillary skimmer-cone regions that are often incorporated into ESI source designs.[54]

Pathway c represents still another configuration that is often used to record ion mobility data. Here, the ion trap is enabled and is used to accumulate and then inject ions into the drift tube. In this configuration, the TOF region is disabled, and ions are detected on-axis (as in path a). At low OSC voltages (and without m/z selection in the quadrupole), we obtain the ion mobility distribution of the ions from the source. By fixing the quadrupole to pass a narrow m/z range, we can obtain a selected ion mobility distribution. Finally, fragments generated at high OSC voltages can be selected by the quadrupole. In this configuration, it is possible to examine the origins of each fragment ion. This approach is similar to a traditional MS/MS configuration that is often referred to as a product ion scan, an approach that allows one to determine the m/z values for all parents that can give rise to a specific fragment ion. Similarly, we can use the capabilities in path c to determine the mobilities for all parents that give rise to fragments with a specific m/z value. The latter experiment is an important complement to MS methods, because it provides a means of determining which isomers or conformers give rise to a specific fragment.

Finally, path d shows a number of experiments that can be carried out upon enabling the TOF region. At low OSC potentials, this configuration can be used to obtain nested $t_D(t_F)$ distributions for parent ions. An important feature of the present configuration is the ability to induce fragmentation for distributions of ions as they exit the drift tube. This can be carried out by increasing the OSC potential or by addition of a collision gas to the octopole

(53) Morris, H. R.; Paxton, T.; Dell, A.; Langhorne, J.; Berg, M.; Bordoli, R. S.; Hoyes, J.; Bateman, R. H. *Rapid Commun. Mass Spectrom.* **1996**, *10*, 889. Shevchenko, A.; Chernushevich, I.; Ens, W.; Standing, K. G.; Thomson, B.; Wilm, M.; Mann, M. *Rapid Comm. Mass Spectrom.* **1997**, *11*, 1015.

(54) See, for example: Smith, R. D.; Loo, J. A.; Barinaga, C. J.; Edmonds, C. G.; Udseth, H. R. *J. Am. Soc. Mass Spectrom.* **1990**, *1*, 53. Katta, V.; Chowdhury, S. K.; Chait, B. T. *Anal. Chem.* **1991**, *63*, 174. Lowery, K. S.; Griffy, R. H.; Kruppa, G. H.; Speir, J. P.; Hofstadler, S. A. *Rapid. Commun. Mass Spectrom.* **1998**, *12*, 1957. van Dongen, W. D.; van Wijk, J. I. T.; Green, B. N.; Heerma, W.; Haverkamp, J. *Rapid. Commun. Mass Spectrom.* **1999**, *13*, 1712.

Table 2. Summary of Several Assigned Parents and Fragments from Parallel CID of β-casein Tryptic Digest

z[a]	position[b]	$t_D(t_F, m/z)$[c]	assigned fragments[d]
1	41−43	2.72(24.46, 374.5)	*y_2*, $b_2 + H_2O$, *$y_2 - NH_3$*, b_2, y_1
	45−47	2.78(24.94, 389.3)	y_2, $y_2 - H_2O$, *b_2*, *$b_2 - H_2O$*, y_1
	41−44	3.54(28.29, 503.0)	*y_3*, *$y_3 - NH_3$*, b_3, *y_2*, *$y_2 - NH_3$*, *$b_2 + H_2O$*, y_1
	44−47	3.43(28.70, 517.3)	y_3, *372.0*, y_2, $y_2 - H_2O$, *b_2*, y_1
	115−120	3.89(32.04, 646.0)	y_5, y_4, b_4, a_4, AMAP − 28, b_3, y_3, a_3, y_2, b_2
	218−224	4.30(34.32, 742.5)	y_5, b6, a_6, b_5, a_5, y_4, b_4, PII, b_3, *FP/PF*, *PI*, *PI − 28*, b_2
	123−128	4.30(34.45, 748.8)	y_5, a_5, b_4, y_4, y_3, b_3, b_2, *FP/PF*, y_2, a_2
	185−191	4.54(35.18, 780.8)	y_5, *LPVPQ − NH_3*, y_3, b_3, a_2, b_2
	192−198	4.42(36.28, 830.2)	y_5, b_6, $b_6 - NH_3$, a_6, *VPYPQ*, *VPYPQ − 28*, *VPYPQ − NH_3*, b_5, a_5, *VPYP*, *VPYP − 28*, YPQ, *YPQ − NH_3*
	121−128	5.12(40.04, 1013.5)	y_6, a_6, *KEM*
	113−122	5.41(42.40, 1138.4)	y_7, *764.9*, *EAMAPKH − NH_3*, y_6, EAMA − 28, *y_2*
2	121−128	2.78(28.43, 507.2)	y_7, b_6, y_6, a_6, b_3, y_3, *EM*, *244.03*, *EM − 28*, y_1
	113−122	2.90(30.10, 570.0)	*EAMAPKH − NH_3*, APKH, *PK*, $b_2 - NH_3$, PK − NH_3, 197.8, EA − H_2O, y_1
	48−63	4.13(39.63, 991.1)	*244.0*, y_2, *375.2*, $y_4 - H_2O$, 488.2, b_4, y_4, EEQQ, 597.5, 625.2, 843.2, 1082.7, *1089.0*, y_{10}, *1327.0*, $y_{12} - H_2O$, a_{13}, $b_{13} - NH_3$, 1688.1
	*48−63	4.01(40.40, 1032.0)	QD − H_2O, *244.0*, QTE − 28, *374.2*, sEEQQQ − NH_3, EEQQQTE − H_2O, QTEDELQD − H_2O, *955.4*, sEEQQQTE − NH_3, EEQQQTEDE − 28, *EQQQTEDELQ − 28*, EEQQQTEDELQ − NH_3
	*44−63	4.71(44.95, 1280.6)	LQD − H_2O, $y_6 - H_2O^{2+}$, $y_3 - H_2O$, y_3, 457.9, IEKF, 585.2, $b_{10} - NH_3^{2+}$, TEDELQD − 28, 860.1, y_7, 971.1, $b_{17} - H_2O^{2+}$, 1326.0, FQsEEQQQTED − 28, 1412.1, 1566.4
	*16−40	5.53(49.56, 1560.7)	Vesls − 28, 742.1, NVPGEIVE − NH_3, VesLss, EIVEsLs, 980.6, a_{17}^{2+}, y_{19}^{2+}, PGEIVEsLss − 28, LNVPGEIVEsL − NH_3, 1234.4, NVPGEIVEsLs, $y_{11} - H_2O$, ELNVPGEIVEsLs, PGEIVEsLsssEE − H_2O, GEIVEsLsssEESI − 28
	*16−43	5.94(52.28, 1738.7)	y_7, 1341.0, LNVPGEIVEsLs − 28, 1469.9, EELNVPGEIVEsLs − 28

[a] Parent ion charge state. [b] Position of the assigned tryptic fragment in the protein sequence: (15-RELEELNVPGEIVESLSSSEESITRINKKIEKFQ-SEEQQQTEDELQDKIHPFAQTQSLVYPFPGPIPNSLPQNIPPLTQTPVVVPPFLQPEVMGVSKVKEAMAPKHKEMPFPKYPVEPFTESQSLTLTDVE-NLHLPLPLLQSWMHQPHQPLPPTVMFPPQSVLSLSQSKVLPVPQKAVPYPQRDMPIQAFLLYQEPVLGPVRGPFPIIV). The asterisks (*) indicate peptides in which serine residues are phosphorylated. [c] Parent ion experimental drift time and flight time [ms(μs)] and calculated m/z ratio. [d] Fragment assignments are consistent with ref 47. In cases where multiple fragment assignments are possible, only the m/z is given. Assignments shown in italics are not unambiguously ascribed to one parent ion.

collision cell. In the discussion of β-casein given above, we showed that it is possible to induce fragmentation of a relatively large number of peptides. The dissociation profile of all ions in a single experimental sequence is extremely complex; however, the mobility separation simplifies this distribution; in many cases it is possible to interpret fragmentation data because only a few parent ions dissociate over a narrow drift time range.

Path d also shows configurations in which the quadrupole is enabled. At low OSC potentials, this configuration is essentially a Q-TOF instrument that has been equipped with a front-end ion mobility spectrometer. This configuration is useful for simplifying fragmentation data that are found when multiple ions have identical mobilities. That is, in such a case, the quadrupole can be used to select a narrow m/z range for CID studies. Finally, we have demonstrated several additional capabilities that arise upon incorporating two fragmentation processes, high OSC potentials followed by activation in the octopole collision cell. Generation of 1° fragments in the OSC region can remove the strong correlations of drift times and flight times. This increases the peak capacity of the measurement and simplifies m/z selection, since in many cases, it is possible to select 1° fragment ions that fall at unique positions in the $t_D(t_F)$ datasets. We demonstrated this approach above by examining several peptide systems.

SUMMARY AND CONCLUSIONS

We have described the development of a combination of ion mobility separations, collisional activation, and multiple stages of MS for the analysis of complex peptide mixtures. Two ideas were carefully considered in the development of these hybrid techniques. First, the time scales associated with collisional activation were initially kept short (<100 μs) such that it is possible to record datasets using the nested drift(flight) time acquisition scheme described previously.[19] In this way, the mobility separation that occurs in the drift tube is not compromised by the subsequent activation processes. Second, by incorporating an activation technique at the back of the drift tube (i.e., the OSC region), it is possible to generate 1° fragments that can subsequently be selected in the quadrupole and exposed to energizing collisions, and then distributions of 2° fragments can be analyzed in the TOF mass spectrometer. A fundamental limitation in the use of mobility/TOF techniques is that the sizes and masses of ions are correlated; because of this, mobilities and m/z ratios are not entirely independent. The ability to generate fragment ions at the exit of the drift tube creates ions with new m/z ratios. Although the 1° fragments are also coincident in drift time with the original parent ions, their new m/z ratios are not correlated with the size of the parent. This effectively increases the peak capacity that is used in the nested drift(flight) time experiment by dispersing peaks at a given drift time over a substantially greater m/z range.

We also note that although improvements in sensitivity have been demonstrated, the current technologies are still not as sensitive as the well-developed MS/MS strategies; however, we believe that much of this difference will be diminished as additional improvements in the instrumental efficiencies are made. This type of work is ongoing in our laboratory.[55] Finally, the time scales of these techniques are suitable for coupling with condensed-phase separation methods; we are currently in the process of developing an LC interface for the present instrument.[52]

(55) Myung, S.; Lee, Y. J.; Clemmer, D. E. Work in progress.

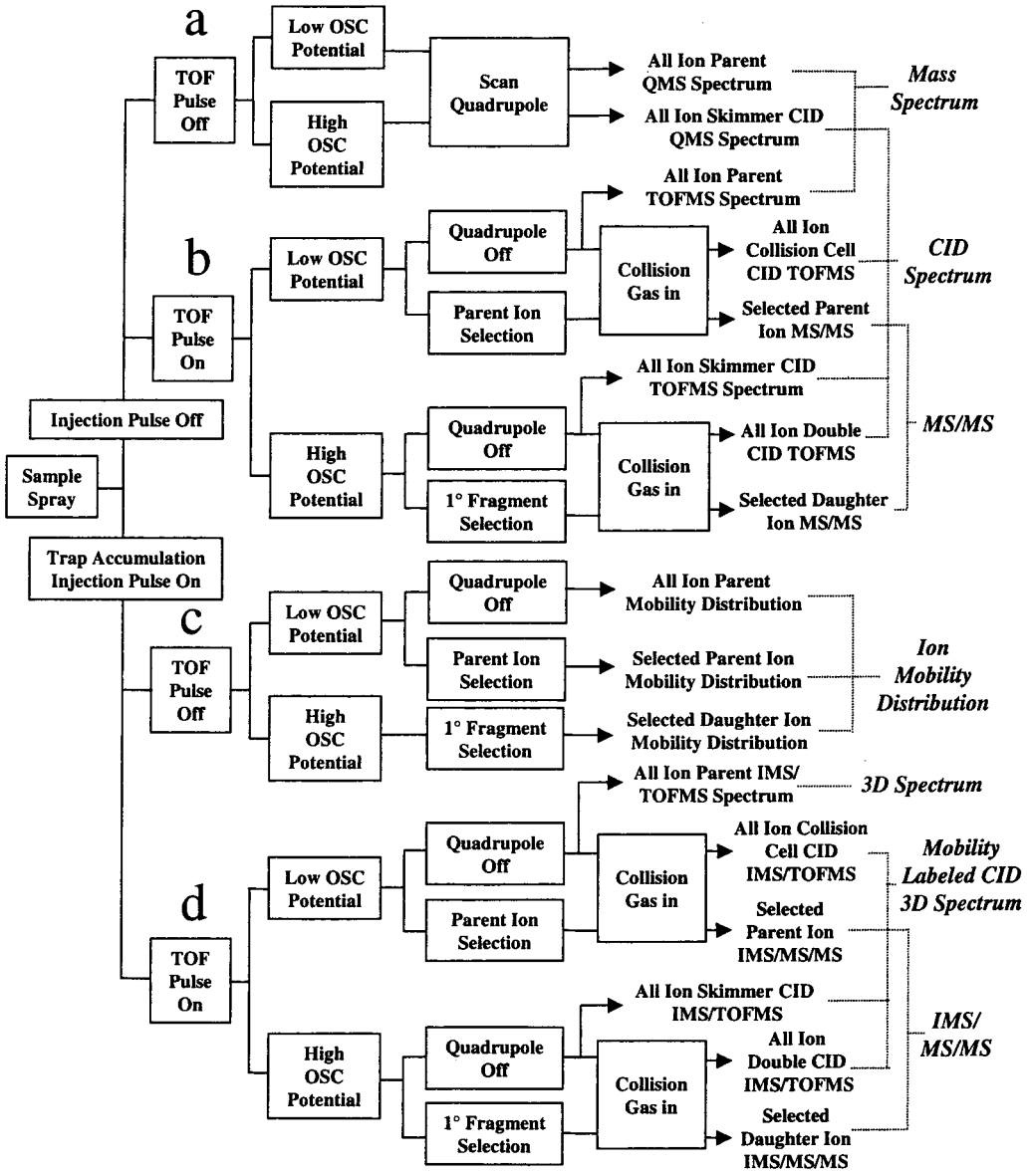

Figure 8. Flow diagram of the experimental approaches commonly employed with the current instrumental configuration shown in Figure 1. See text for details.

ACKNOWLEDGMENT

This work was supported by a grant from the National Institutes of Health (1R01GM-59145−01). We also acknowledge supplemental support of this project from the Camille and Henry Dreyfus foundation. C.S.H.−H. gratefully acknowledges generous support from an American Chemical Society Division of Analytical Chemistry Graduate Fellowship sponsored by Merck & Co. We are grateful for critical comments from Catherine Srebalus Barnes, Milos Novotny, Gary Hieftje, and James Reilly as well as other reviewers of our manuscripts who continue to encourage us to improve these techniques.

Received for review July 24, 2001. Accepted December 21, 2001.

AC010837S